Measurement of the $pp \to pp\pi^0$ reaction at 850 MeV/c and partial wave cross sections

M. Betigeri,[9] J. Bojowald,[1] A. Budzanowski,[4] A. Chatterjee,[9] J. Ernst,[7] L. Freindl,[4] D. Frekers,[8] W. Garske,[8] K. Grewer,[8] A. Hamacher,[1] J. Ilieva,[1,5] L. Jarczyk,[3] K. Kilian,[1] S. Kliczewski,[4] W. Klimala,[1,3] D. Kolev,[6] T. Kutsarova,[5] J. Lieb,[10] H. Machner,[1] A. Magiera,[3] R. Maier,[1] H. Nann,[11] J. Niskanen,[12] D. Prasuhn,[1] L. Pentchev,[5] D. Protić,[1] B. Razen,[1] P. von Rossen,[1] B. J. Roy,[9] R. Siudak,[4] A. Strzałkowski,[3] R. Tsenov,[6] and K. Zwoll[2]

[1]*Institut für Kernphysik, Forschungszentrum Jülich, Jülich, Germany*
[2]*Zentrallabor für Elektronik, Forschungszentrum Jülich, Jülich, Germany*
[3]*Institute of Physics, Jagellonian University, Krakow, Poland*
[4]*Institute of Nuclear Physics, Krakow, Poland*
[5]*Institute of Nuclear Physics and Nuclear Energy, Sofia, Bulgaria*
[6]*Physics Faculty, University of Sofia, Sofia, Bulgaria*
[7]*Institut für Strahlen- und Kernphysik der Universität Bonn, Bonn, Germany*
[8]*Institut für Kernphysik, Universität Münster, Münster, Germany*
[9]*Nuclear Physics Division, BARC, Bombay, India*
[10]*Physics Department, George Mason University, Fairfax, Virginia*
[11]*Physics Department, Indiana University, Bloomington, Indiana*
[12]*Department of Physics, University of Helsinki, Finland*

(Received 21 August 2001; revised manuscript received 19 February 2002; published 23 May 2002)

A stack of annular detectors made of high purity germanium was used to measure $pp \to pp\pi^0$ differential cross sections at a beam momentum of 850 MeV/c. A total cross section of $\sigma = 9.1 \pm 1.1$ μb is deduced. The fitted distribution of different partial waves to the world total cross section data and to the present differential cross sections favors an approach without low-energy approximations, with the standard value for the final state interaction scattering length, and an important contribution from an intermediate $N\Delta$ state.

DOI: 10.1103/PhysRevC.65.064001 PACS number(s): 13.75.Cs, 25.40.Qa

I. INTRODUCTION

With the advent of accelerators producing beams of high brilliance and very low-energy spread the threshold regions in light meson production became accessible. The π^0 production is the first inelastic channel that opens in proton-proton interactions and is therefore of fundamental importance. It was a great surprise when the first new data for this reaction emerged [1] and the total cross sections were found to be a factor of 7 larger than the theoretical predictions available at that time [1,2]. Since then, intense theoretical activity started (for a review see Ref. [3]). The bulk of total cross section data are from only two groups, one at the IUCF cooler ring and one at the Celsius accelerator in Uppsala. While the Uppsala group concentrated on differential and total cross sections [4–6], the IUCF group employed polarized proton beams and also a polarized proton target [7–9] allowing the measurement of spin correlation coefficients. These latter measurements are only relative ones, thus no total cross section was extracted. The Saclay group [10] covered a large energy range with one beam momentum very close to that of the present experiment.

To summarize the situation: total cross sections exist in the range from 278.0–325.0 MeV from Ref. [1], 280.7–310.2 MeV from Ref. [4], 310 MeV from Ref. [5], and 310–425 MeV from Ref. [6]. The latter data are slightly larger than those from Meyer *et al.* [1]. The data from Ref. [10] range from 325–1012 MeV with only one measurement below $\eta = 1$.

II. EXPERIMENT

In order to investigate the mentioned disagreement we have measured the π^0 production at a beam momentum of 850 MeV/c corresponding to an energy of 327.77 MeV which is slightly above the highest data point from the IUCF group. This point was measured simultaneously with the $pp \to d\pi^+$ reaction [11]. Since the collected luminosity was optimized for this reaction, which has a larger cross section, the data of the present reaction suffer from poor statistics. In what follows we will discuss pertinent experimental details but additional information is given in Ref. [11]. The external beam from the COSY accelerator in Jülich was focussed onto a thin liquid hydrogen target. Details will be given below. The reaction particles were detected by a stack of three segmented germanium detectors called the germanium wall [12]. All detectors have a hole in their respective centers allowing the beam to exit to the magnetic spectrograph BIG KARL [13]. The first detector (quirl) is position sensitive by segmentation with 200 Archimedes spirals on the front and rear side with opposite orientation. Each spiral from the front side crosses a spiral from the rear side, thus defining 40 000 pixels. This quirl detector is 1.3-mm thick with a 5.8-mm diameter hole in the center. It was followed by two detectors (pizzas) segmented into 32 wedges each. Each of these pizza detectors is 17-mm thick. The whole setup stopped protons up to 129 MeV completely. It accepts particles emitted between 50 and 280 mrad. The energy resolution of these detectors was better than 4×10^{-4}. A 2-mm-thick plastic scintillator with dimensions of 30 cm$\times$40 cm with a 4-mm diameter hole in its middle was mounted 6-cm upstream as a

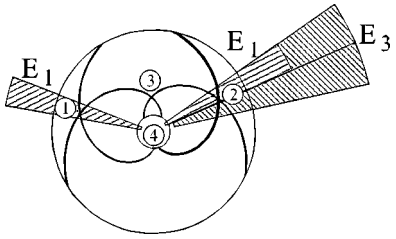

FIG. 1. The identification of a two hit event in the germanium wall (see text). Shown are the four spirals having fired in the quirl detector. The wedges from the downstream detector $E1$ with coincident signals are indicated as hatched areas. Also shown are the coincident wedges from detector $E3$, where two neighboring segments had fired.

veto counter. All detector elements as well as the target cell were aligned on the beam axis with the help of an optical telescope which viewed a 90° mirror mounted on a moveable arm behind the quadrupole magnets of the spectrograph.

The focussed beam with a reduced intensity of only $\approx 10^3$ protons per second was steered away from the hole onto the germanium wall. With the help of the quirl detector we could measure its dimensions. Fits of Gaussians to the horizontal and vertical directions yield full widths at half maximum (FWHM's) of 1.55 and 1.25 mm, respectively. A small but possible nonnormal incidence of the beam will lead to an error in the angle measurement. This can result in rather large uncertainties in one arm measurements especially with a magnetic spectrograph [14]. However, the present measurement deals with the relative angle between the two emerging protons, thus this uncertainty cancels out.

Unlike in charged pion production measurements [11], a twofold coincidence was required in the germanium wall. This constraint reduced the background significantly. Two hits in the first double-sided segmented quirl detector produce an ambiguity in the locus, since each Archimedes spiral on the front side crosses all of the rear side. The possible positions of the tracks through the detector are denoted by 1–4 in Fig. 1. Since the following two detectors $E1$ and $E3$ are segmented similar to wedges, possibilities 3 and 4 can be excluded from the hit pattern. Excellent energy resolution allowed unambiguous proton selection. Through the measurement of the four-momentum vectors of both protons it was possible to extract the missing mass of the unobserved π^0. The present reaction at 850 MeV/c beam momentum produces protons with energies up to 154.2 MeV into opening angles up to 392 mrad. This leads to a reduced acceptance for the present reaction when compared to lower beam momenta for the present detector setup because of its limited geometrical acceptance as well as its energy range. This acceptance was studied with Monte Carlo simulations employing the code GEANT [15]. This is illustrated in the lower part of Fig. 2. The input distribution, which is isotropic plus the final state interaction (FSI), is compared with the result of the Monte Carlo calculation. It goes without saying that the input distribution is nicely regained. The final efficiency curve is shown in the upper part of Fig. 2. It should be noted that the effeciency is zero only for $Q \leqslant 0.45$ MeV. Corrections for the reduced efficiency due to nuclear interactions of

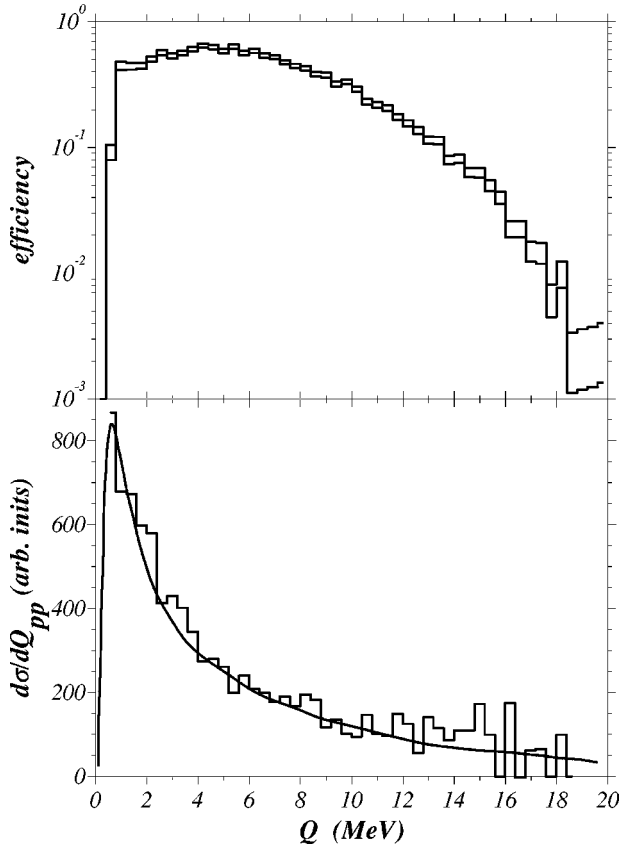

FIG. 2. Upper part: The efficiency of the present setup according to Monte Carlo calculations. The two histograms show the error band. Lower part: Input for the Monte Carlo calculation (an isotropic distribution with FSI employing the standard value for the scattering length) is shown as a solid curve. The result of the Monte Carlo simulation is shown as a histogram (see text for discussion).

the reaction protons with the detector material were performed using the formula given by Machner and Razen [16] yielding a further efficiency reduction between 1 and 0.85.

The target was a cell of 6-mm diameter, a thickness of 6.4 mm, and windows with 1.5-μm thickness. It was filled with liquid hydrogen having a temperature of ≈ 15 K. The length of the target introduced an error in the angle measurement of four times the inherent detector resolution. For the present reaction the angle uncertainty between the two protons is of interest. This leads to errors ranging from 6 to 15 mrad, depending on the emission angles.

The deduced missing mass distribution is shown in Fig. 3. This distribution is the difference of counts from a full target measurement and the counts from an empty target measurement. However, the latter number was small (see Ref. [12]). A Gaussian was fitted to the data yielding a resolution of FWHM$=5.9$ MeV/c^2. The main contribution to the resolution results from the short distance from the target to the germanium wall of only 73 mm which introduced an uncertainty in the emission angle measurements.

The spatial limits of the detector are confirmed by plotting the data in a Dalitz plot (Fig. 4). The lack of events in the lower left part of the allowed region is due to the limited acceptance of the detector as discussed above. A small in-

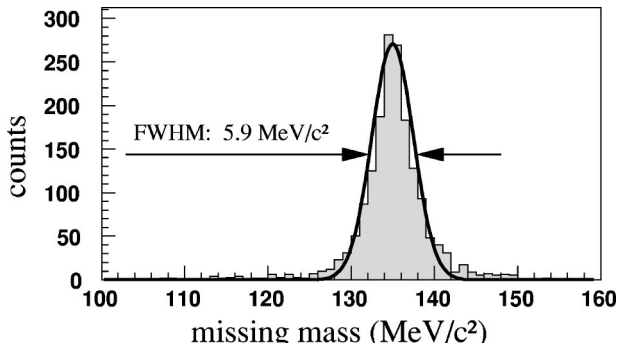

FIG. 3. Missing mass distribution of the reaction $pp \to pp\pi^0$ with two detected protons. The data are shown as a histogram and the Gaussian fit as a solid curve. Negative counts from empty target subtraction are suppressed.

variant mass corresponds to the small energy in the proton-pion system and hence to a large momentum of the other proton relative to this system. The missing yield in the upper right part of the plot corresponds to events with a small relative momentum between the two protons which are emitted close to the beam direction. These particles could not be detected because of the hole in the germanium wall which allows the primary beam to exit. The enhancement of events close to this hole is due to the strong proton-proton final state interaction (FSI).

The luminosity was determined by measuring the target thickness, the density of the liquid hydrogen, and the number of incident protons. The target thickness was measured with an optical telescope mounted on a micrometer thread. The beam intensity was deduced from a measurement of scattered particles by detectors which were calibrated by a separate

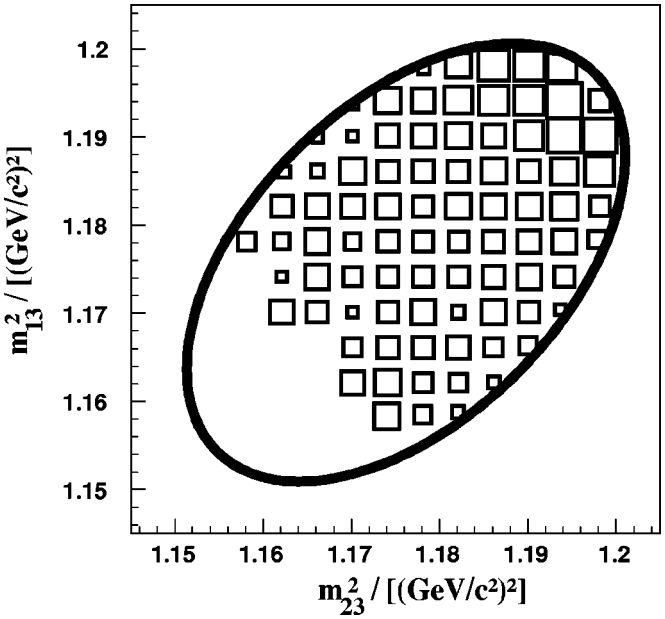

FIG. 4. Dalitz plot of the efficiency corrected data. $m_{1,2}$ denotes the protons and m_3 denotes the pion. The area of the squares is proportional to the number of events. The solid curve is the kinematical limit.

measurement, in which the scattered particle intensity was measured as function of the beam intensity (see Ref. [11]). The advantage of this method compared to elastic scattering is that the monitor counters can be at positions where the counting rate is large. No precise knowledge of the scattering angle or the solid angle of the monitor counters is necessary. It does not depend on other measurements with their inherent errors. Finally, the setup allowed also the measurements of cross sections in reactions with other target-projectile combinations without readjustment of the counters [14] after proper calibration. In the present experiment a total luminosity of $(8.0 \pm 0.6) \times 10^{32}$ cm^2 was collected within 7 h.

III. THEORETICAL CONSIDERATIONS

A. Cross section

The cross section for the present reaction is given by

$$\sigma(Q_{\max}) = \frac{1}{4sp_p^*} \int_0^{Q_{\max}} |T(Q)|^2 q(Q) p(Q) dQ, \qquad (1)$$

with $p(Q)$ the proton momentum in their center-of-mass system, $q(Q)$ the pion center of mass momentum relative to the two-proton system, and Q the energy in the energy between the two protons. In deriving Eq. (1) relativistic relations were applied. The differential cross section with respect to the energy is then

$$\frac{d\sigma}{dQ} = \frac{1}{4sp_p^*} |T(Q)|^2 q(Q) p(Q). \qquad (2)$$

In order to study the momentum dependence of the matrix element

$$T = \langle \Psi_f | V | \Psi_i \rangle \qquad (3)$$

we first assume plane waves in the entrance and exit channels, respectively. Deviations from this approach are then accounted for by initial and final state interactions. Since the proton beam energy is rather large, the former can reasonably be ignored. Also the pion-proton interaction in the final state is weak and can be ignored. The plane waves can be expanded in terms of partial waves. The radial part, which is momentum dependent, is then

$$T_{L_i,Ll} = \sqrt{a_{L,l}} \langle j_L(pr) j_l(qr/2) | V(r) | j_{L_i}(p_p^* r) \rangle \qquad (4)$$

with L_i, L, and l denoting the angular momenta of the incident two-proton system, the final two-proton system, and the one between the pion relative to the final two-proton system, respectively. The constants $a_{L,l}$ contain all other dependencies. The ''potential'' was assumed to be of a Yukawa form

$$V(r) \propto e^{-\mu r}/r, \qquad (5)$$

with $\mu = (\sqrt{3}/2) m_\pi / (\hbar c)$ from the pion rescattering approach given by Koltun and Reitan [17]. This term is used as a representative illustration for the transition matrix. It is worth noting that in threshold s-wave pion production, it is

TABLE I. The threshold dependence of partial wave amplitudes on the corresponding momenta as a function of the angular momenta. The dependence of the matrix element and the partial cross sections on $\eta = q_{\max}/m_\pi$, given by the barrier penetration model $\sigma_{L,l} \propto \eta^m$ is also given.

L_i	initial state	$L_{N\Delta}$	final state	L,l	$\lvert T_{L,l}\rvert$	m
1	$^3P_0$	1	$^1S_0 s_0$	0,0	1	4
1	$^3P_2$	1	$^1S_0 d_2$	0,2	q^2	8
0	$^1S_0$	2	$^3P_0 s_0$	1,0	p	6
1	$^3P_{0,1,2}$	1	$^3P_{0,1,2} p_{0,1,2}$	1,1	pq	8
1	$^3P_2$	1	$^1D_2 s_2$	2,0	p^2	8
2	$^1D_2$	0	$^3P_2 s_2$	1,0	p	6
3	$^3F_{2,3}$	1	$^3P_2 p_{2,3}$	1,1	pq	8

the dominant mechanism (perhaps together with a structurally similar heavy meson exchange).

Integration of Eq. (4) and insertion into Eq. (1) leads to the total cross section while the integrand is the differential cross section. In the following we will refer to this model as the full model (FM). In Table I we compile the allowed transitions with $L_i \leqslant 3$ and $L,l \leqslant 2$ (of higher partial waves only the most important are shown). The usual spectroscopic notation $^{2S+1}L_j l_J$ is applied with S and j denoting the spin and total angular momentum in the final two-proton system, respectively, and J the total angular momentum. Since the energy dependence is a function mainly of the final state [see Eq. (4)] and hence cannot distinguish the initial states of the listed transitions, we restrict the fitting procedure discussed below to only the transitions labeled by the final orbital angular momenta, considering it to be an analysis of final states rather than initial ones. In this table we also give the angular momentum between the nucleon and the Δ in the most important (or only) intermediate $N\Delta$ states.

The Δ is strongly excited when its orbital angular momentum is smaller than for the corresponding NN partial wave. In this case the energy lost in the mass barrier is regained with the decrease in the centrifugal energy and one can get a resonance-like behavior as shown in Ref. [18] for isospin 1 ''dibaryons.'' Reference [19] also obtained a resonant behavior in the present reaction for the transition $^3F_2 \rightarrow Sd$ [through the intermediate states $^3P_2(\Delta N)$ and $^5P_2(\Delta N)$], although this contribution to the total cross section was estimated to be very small. Also experimentally this amplitude was found to be rather small [5]. However, Ref. [19] considered only S-wave final nucleons. Releasing this constraint makes the above Δ contribution much more important. For example, for the above initial state the final state $^3P_2 p$ is much larger, getting a significant contribution from the $N\Delta$ intermediate states. With equal or higher angular momenta of the $N\Delta$ the effect of Δ excitation is much less important with no resonant behavior as first seen explicitly in $pp \rightarrow d\pi^+$ [20] and in Ref. [18]. On the other hand, the experimental excitation function shows an enhancement in the vicinity of $\eta = 1.8$. From this point of view Ps and and even more Pp final states may get a large contribution from Δ excitation. This point will be discussed further in Sec. IV.

B. Low-energy approximation

For the case of the near threshold region several approximations can be made. First, the Bessel functions can be approximated for small arguments x by

$$j_l(x) = \frac{x^l}{(2l+1)!!}. \tag{6}$$

Insertion into Eq. (4) leads after integration to momentum dependencies

$$T_{L_i L l} \propto p_p^{*L_i} p^L q^l. \tag{7}$$

The second approximation is the nonrelativistic treatment in Eq. (1). The total cross section for the related reaction $pp \rightarrow d\pi^+$ can be fitted by assuming $l \leqslant 2$ for $\eta \leqslant 3$ [21]. We, therefore, restrict the analysis to the same angular momenta. This leads to the transitions given in Table I and in the threshold approximation of Eq. (7) to the dependencies given in the last column of Table I.

The third approximation is to neglect the variation in p_p^* and in the total c.m. energy. The integration can then be analytically performed leading to a relation $\sigma_{L,l} = a_{L,l}\eta^m$ with $\eta = q_{\max}/m_\pi$, which is known as the barrier penetration model [22,23]. The dependence for the Ss channel is strongly modified by the final state interaction leading to a dependence closer to $\sigma_{Ss} \propto \eta^2$. This collection of approximations will be called in the following the low energy approximation (LEA).

C. Final state interaction

It is a common practice to separate the amplitude for meson production in nucleon-nucleon collisions into a meson production amplitude and a final state interaction. The former is assumed to be only weakly energy dependent, thus yielding mainly the dependencies given in Table I. Another common approximation is to assume the meson interaction with the two-nucleon system to be rather weak. The final state interaction thus reduces to the nucleon-nucleon interaction. For energies close to the threshold it is normal to treat the energy dependence due to the final S-wave interactions between the two nucleons in a factorization approximation

$$\lvert T_{Ss}\rvert^2 \propto \lvert T_{0,0}\rvert^2 \lvert T_{\mathrm{FSI}}\rvert^2 \tag{8}$$

with $T_{0,0}$ from Table I.

The FSI matrix element is calculated according to the modified Cini-Fubini-Stranghellini formula [24] and using the usual Gamow Coulomb correction factor C_0. A scattering length of $a_{pp} = -7.83$ fm and an effective range $r_0 = 2.8$ fm are used. The shape parameters used are the standard values [24]. Essentially the large scattering length causes the low-energy behavior of the Ss final state to become closer to η^2 than η^4 of Table I (and Sd to η^6).

Meyer *et al.* [9] found an effective scattering length of -1.5 fm instead of the accepted value of -7.82 fm necessary, in order to reproduce the pion angular distributions. We will come back to this issue later.

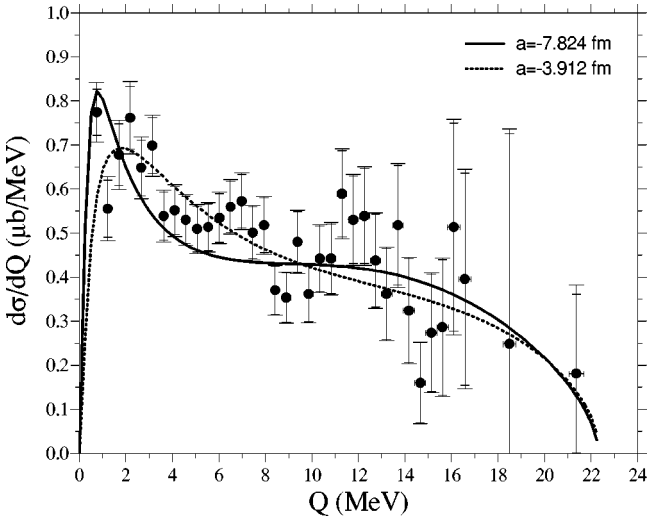

FIG. 5. $d\sigma(Q)/dQ$ for the present experiment as function of the energy Q in the two-proton system is shown as full dots. The error bars in the cross sections with the small crossbars represent the statistical error only and the one with the large crossbar is the sum of the statistical error and the uncertainty of the efficiency correction added in quadrature. Also shown are two fitted distributions with the normal value of the Fermi scattering length ($a = -7.824$ fm) as a solid curve and the one with half of this scattering length as a dashed curve.

The validity of the present approach of factorizing the matrix element into an almost momentum independent production element and a strongly momentum dependent one for the FSI was recently questioned [25,26], because for direct production (impulse term) in the absence of any interaction $V(r)$, the other factor $|T_{0,0}|^2$ should be very close to zero. However, it was also pointed out in Ref. [26] that the energy dependence from the above FSI is correct even for this term, and that is the purpose for which this FSI effect is used in the present work.

IV. RESULTS AND DISCUSSION

In Fig. 5 we show the efficiency corrected distribution from the present measurement as a function of the energy in the two-proton system Q. The uncertainty in the cross sections due to statistics and due to the efficiency correction are shown separately. Also shown is the error in the measurement of the relative proton energy. This error stems mainly from the uncertainty in the angle measurement due to the relatively large target with respect to the short distance of only 73 mm between the target and the germanium wall. The statistics especially for $Q > 12$ MeV is meager. The reason is the small collected luminosity due to reasons pointed out above.

From the total number of efficiency corrected counts, target thickness, beam current, and dead time correction of the data acquisition system the total cross section was found to be

$$\sigma = [9.1 \pm 0.80 \ \text{(stat.)} \pm 0.75 \ \text{(syst.)}] \ \mu\text{b}. \qquad (9)$$

TABLE II. Fractional contributions of the different partial waves as a function of the scattering length from fitting the differential distribution. The first three lines show the fit of all three partial waves, the last three lines those with the Ps strength fixed at a value derived from the spin correlation coefficient measurement (Ref. [9]).

scattering length	Ss	Ps	Pp	model
−7.824 fm	0.56±0.04	0.07±0.19	0.37±0.19	LEA
−7.824 fm	0.53±0.02	0.02±0.08	0.46±0.08	FM
−3.912 fm	0.73±0.03	0.24±0.08	0.03±0.08	FM
−7.824 fm	0.51±0.03	0.23±0.02	0.26±0.03	LEA
−7.824 fm	0.53±0.03	0.23±0.02	0.24±0.05	FM
−3.912 fm	0.73±0.03	0.23±0.02	0.04±0.04	FM

The cross section and the quoted statistical error are obtained by fitting the different model functions to the data as shown in Fig. 5 and finally integrating these functions. Absolute normalization [beam intensity (± 0.455 μb) and target thickness (± 0.455 μb)] and empty target subtraction (± 0.38 μb) are the main contributions to the systematical error. Efficiency correction and dead time correction lead to negligible contributions. These contributions are added in quadrature. If the statistical and the systematical errors are also added in quadrature, a total uncertainty of ± 1.1 μb is obtained.

The yield of the Ss wave with the properly chosen FSI is responsible for the maximum around 1 MeV. A pure Ss wave cannot account for the data. The Pp wave yield has a maximum around 10 to 12 MeV while the Ps wave has one around 18 to 20 MeV. The Ds wave is in between these two waves. This wave as well as Sd and Dp were found to give negligible contributions to the cross section in the present energy range [27].

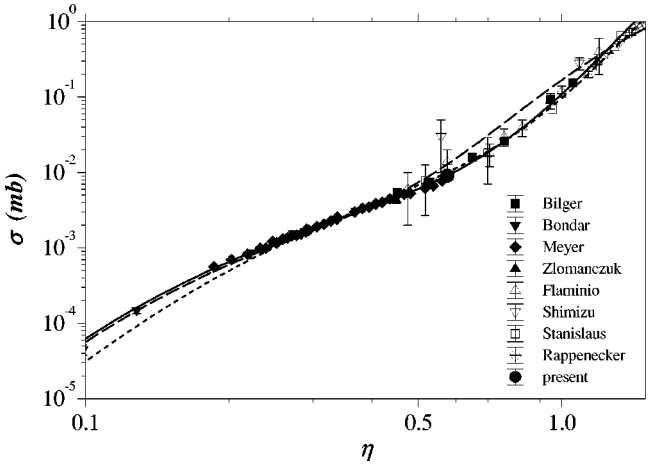

FIG. 6. Excitation function. Older data are from Refs. [28–30] and the newer from Refs. [1,4–6,10]. The present measurement is indicated by a thick dot. The dashed curve is the fit of the model employing the Yukawa equation (5). The solid curve shows the fit with Δ excitation and the standard value of the proton-proton scattering length. Changing this value to one half yields the dotted curve.

TABLE III. Constants $a_{L,l}$ as derived from the fits of the low-energy approximation (LEA) and the full model (FM) to the total cross section. The a_{Ps} coefficients are obtained from fitting the cross sections as obtained from spin correlation coefficients [8,9]. The $a_{L,l}$ are given in units of mb.

Model	Scattering length	a_{Ss}	a_{Ps}	a_{Pp}
LEA	-7.824 fm	$(1.52\pm0.02)\times10^{-2}$	$(3.30\pm0.16)\times10^{-2}$	$(3.91\pm0.09)\times10^{-2}$
FM, no Δ	-7.824 fm	$(2.16\pm0.08)\times10^{5}$	$(2.02\pm0.16)\times10^{8}$	$(0.945\pm0.035)\times10^{11}$
FM, with Δ	-7.824 fm	$(2.42\pm0.03)\times10^{5}$	$(2.02\pm0.16)\times10^{8}$	$(1.66\pm0.09)\times10^{11}$
FM, with Δ	-3.912 fm	$(5.06\pm0.10)\times10^{5}$	$(2.02\pm0.16)\times10^{8}$	$(1.78\pm0.18)\times10^{11}$

A fit of the three dominating final waves Ss, Ps, and Pp to the data employing Eq. (2) is shown in Fig. 5. Here, the standard value of the FSI scattering length (-7.824 fm) was applied. It follows the general trend of the data, but fails in some details. Notably, there is the sharp low-energy maximum which is not so pronounced in the data. Previous experiments could not measure such small relative energies, because of acceptance cuts of internal experiments due to the beam pipe of the accelerator and due to limited spatial resolution of the detectors employed. We, by way of example, changed the Fermi scattering length to one half of its standard value to move the maximum. The corresponding fit is also shown in Fig. 5. The partial cross sections are given in Table II. The quality of the present data do not allow one to favor one calculation over the other. The same findings are obtained for the low-energy approximation employing Eq. (7). A value of only -1.5 fm for the scattering length as was employed in Ref. [9] can be excluded. It is interesting to note that the fit employing the standard value of the FSI scattering length yields a negligible Ps contribution, independent of whether the full model or the low-energy approximation of it are applied. This is in contrast to recent findings from spin correlation coefficient measurements [8,9]. In contrast, the fit with half of the standard value yields a negligible Pp contribution. We, therefore, make use of the spin dependent results as a constraint on the Ps strength and have adopted the following procedure. First, we have fitted a smooth function to the total cross sections for η values in the vicinity of those of the spin correlation coefficient measurements. These measurements yielded only relative cross sections. With these two inputs the excitation function of Ps for an η interval is derived and the Ps contribution is derived by fitting its energy dependence from the above discussed approach to the data. With this constraint the fit was repeated with almost identical results for FM and LEA employing the same value of the FSI scattering length (lines 4 and 5 in Table II). Only these fits yield all three components with non-negligible values.

Although the two models agree for the present data, they have different momentum dependencies for the different partial waves. We thus study the excitation function of the total cross sections with the hope of distinguishing between different assumptions for the FSI scattering length. The present total cross section is shown together with those from Refs. [1,4–6,10,28–30] in Fig. 6 as a function of $\eta=q_{\max}/m_{\pi}$. The present beam momentum is slightly larger than the last datum from the IUCF group and the datum of the Saclay group also taken at a slightly smaller beam momentum.

As a first step to determining the differential distributions, we fitted the contributions of the relevant partial waves within the barrier penetration model

$$\sigma(\eta)=a_{Ss}|T_{\rm FSI}(\eta)|^2\eta^4+a_{Ps}\eta^6+a_{Pp}\eta^8 \tag{10}$$

to the data. Here $|T_{\rm FSI}(\eta)|^2$ is given by

$$|T_{\rm FSI}(\eta)|^2=\frac{\int_0^{Q_{\max}(\eta)}C_0^2T_{\rm FSI}^2p(Q)q(Q)dQ}{\int_0^{Q_{\max}(\eta)}p(Q)q(Q)dQ} \tag{11}$$

with C_0^2 and $T_{\rm FSI}$ as discussed above. The contribution from Ps was again taken from the spin correlation coefficients. If this wave is kept free in the fits, the value of a_{Ps} was reduced in each iteration step to minimize χ^2 until it finally became zero within error bars. Such behavior was also found in the analysis of differential cross sections by Bilger *et al.* [6]. We, therefore, rely on the above discussed constraint. This procedure yielded an excellent fit to the total cross sections.

The low-energy approximation predicts an always increasing cross section with increasing values for η. It is therefore only valid in some range close to threshold. In addition, p_p^* varies, from 360 up to 510 MeV/c for η varying from 0 to 1. The application of the full model seems to be mandatory. However, the fit of the three partial waves yielded too large cross sections in the range $0.6\leqslant\eta\leqslant1.0$, while it underestimates the data for larger η values (dashed curve in Fig. 6). This problem cannot be cured by introducing an additional Sd or Ds wave, which also an actual calculation [27] indicates to be very small. We have, therefore, allowed the Pp wave to couple to the $N\Delta$ system. Phenomenologically this wave then may be assumed to have a similar resonant form

$$|T_{Pp}|^2=a_{Pp}\frac{(\Gamma^2/4)|\langle j_1(pr)j_1(qr/2)|V(r)|j_1(p_p^*r)\rangle|^2}{(\eta-1.6868)^2+\Gamma^2/4} \tag{12}$$

as for the initial state $^3F_2$ in Ref. [19] originally fitted for the final Ss state. However, the pole structure of the $N\Delta$ should be the same, depending only on the initial state and $N\Delta$ quantum numbers. The width was fitted to $\Gamma=0.97\pm0.07$ as compared with the theoretical value 1.02 of Ref. [19]. This resulted into a much better fit. For the normal value of the pp-scattering length the fit is better (solid curve in Fig. 6)

TABLE IV. Fractional distribution of the total cross section at $\eta = 0.575$ to different partial waves as obtained from fits of the indicated models to the world data. Also given is the predicted total cross sections.

scattering length	Ss	Ps	Pp	$\sigma(\mu b)$	model
-7.824 fm	0.824 ± 0.011	0.129 ± 0.013	0.0505 ± 0.0012	9.3 ± 0.2	LEA
-7.824 fm	0.363 ± 0.013	0.173 ± 0.014	0.465 ± 0.017	13.3 ± 0.3	FM, no Δ
-7.824 fm	0.5731 ± 0.023	0.2433 ± 0.019	0.1836 ± 0.020	9.4 ± 0.3	FM, Δ
-3.912 fm	0.591 ± 0.012	0.22 ± 0.02	0.179 ± 0.023	10.4 ± 0.03	FM, Δ

than for the smaller value by a factor of 2 (dotted curve). This choice influences only the near threshold region as expected. We have also tried a value of $a = -1.5$ fm, as applied in Ref. [9]. However, such an assumption fails completely in the low-energy range. In this case the model calculations underestimate the data in the vicinity of $\eta = 0.2$ by one order of magnitude.

The final values for the fitted parameters are given in Table III. To summarize this study we can state that the LEA as well as FM yield an excellent reproduction of the total cross section data, when the normal value of the scattering length is applied and when for FM, a contribution due to Δ excitation is added. We now proceed with a consistency check. The predictions for the total cross section at $\eta = 0.575$ as obtained from fitting the total cross section excitation function are given in Table IV. Only the two best fits, i.e., LEA and FM with the standard value for the FSI scattering length and Δ excitation for the FM, yield a total cross section value compatible with the present experiment. Neglecting the Δ excitation leads to a too large value as is the case for reducing the FSI scattering length. The values for the fractional contributions to different partial waves are also given in Table IV. They can be compared with those in Table II (lower part). Again, ignoring the Δ excitation and reduction of the FSI scattering length leads to incompatible results. Also, the two analyses in the framework of the LEA yield incompatible results. This becomes evident when comparing the predicted distribution with the presently measured one (see Fig. 7). It clearly overestimates the Ss strength while underestimating the two other partial waves. Adding a factor $1/p_p^*$ to the cross section as suggested by Bilger *et al.* [6] is not satisfactory since it is also ignored in the T-matrix elements. Also shown in Fig. 7 are the predicted distributions for the FM with and without Δ excitation. The quality of the present data is not sufficient to distinguish between these two approaches.

This comparison yields the conclusion that only one model with one set of parameters is capable of reproducing the total cross sections as well as the differential cross sections: the FM with Δ excitation and the standard value of the scattering length. The momentum dependence of the three partial waves for this model is shown in Fig. 8. The Ss wave dominates for small momenta while the Pp wave is the largest wave for large momenta. The Ps wave is never dominant. This explains why free fits tend to ignore this wave. The waves saturate which is, for the interval shown, clearly the case for the Ss contribution. Such behavior is of course not possible in the LEA which is also shown in Fig. 8. However, such saturation was found from data analysis as well as from phase shift analysis in the case of the $pp \to d\pi^+$ reaction (see Ref. [21]). The FSI dominates the Ss contribution close

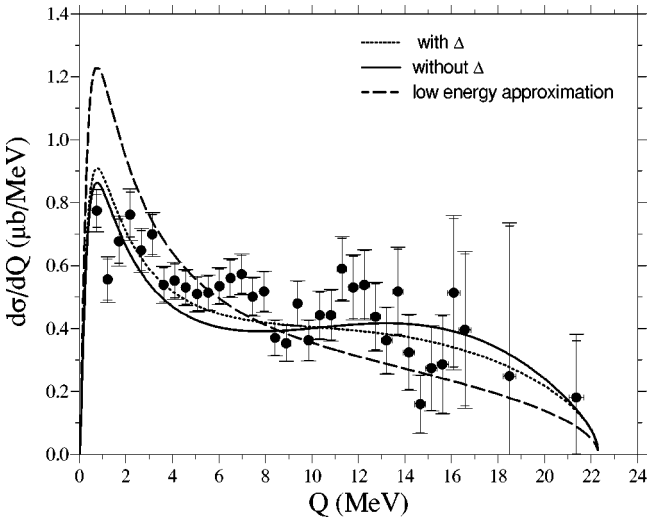

FIG. 7. Same as in Fig. 5. The calculated distributions are for the threshold approximation (LEA) and the full calculation with and without Δ excitation. In all cases the standard value for the FSI scattering length was applied. The fit parameters are given in Table III.

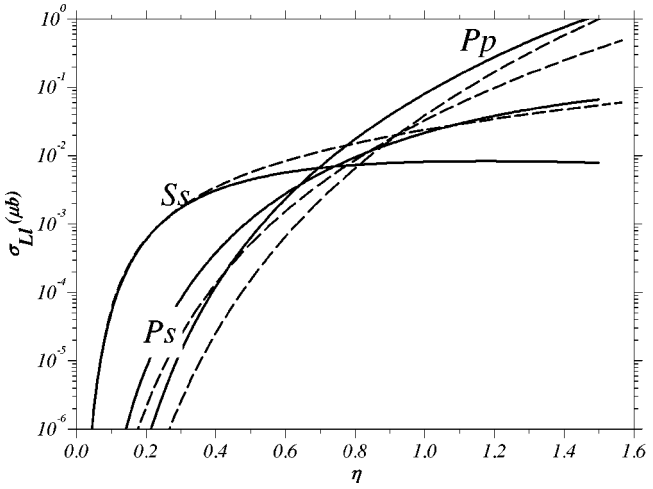

FIG. 8. Excitation function of the three partial waves as obtained from the model fits. The results of LEA with normal value for the FSI scattering length are shown as dashed curves. Those FMs also employing a normal value for the FSI scattering length and a Δ excitation are shown as solid curves.

to threshold and FM as well as LEA agree with each other. Above $\eta \approx 0.3$ the two models diverge. For the other partial waves where no strong FSI exists, the agreement between LEA and FM is worth.

V. CONCLUSIONS

In summary, we have measured differential cross sections as a function of the energy in the final two-proton system. A new value for the total cross section was derived at an energy above the IUCF data points. The cross section was measured absolutely, thus no error due to normalization to simultaneously measured elastic pp scattering occurs. The present cross section is slightly larger than a simple extrapolation of the IUCF data. It is in agreement with the world data as was found by the fits discussed above.

The simple low-energy approximation or barrier penetration model cannot reproduce at the same time the total cross section excitation function and the present differential data. A calculation including the momentum dependencies of the T matrix, relativistic treatment, and the momentum dependence of the incident flux can only reproduce the excitation function when an intermediate $N\Delta$ state is also assumed to contribute, we considered, to the Pp final state. It is noteworthy that its effect is significant in the fit already far below the Δ threshold at $\eta \lesssim 1$ as seen in Fig. 6. The total cross section data at small energies favor the standard value of the FSI scattering length. It is worth mentioning that the present method accounts also for the lowest-energy data which were usually overestimated.

ACKNOWLEDGMENTS

We are grateful to the COSY operation crew for their efforts making a good beam. Support by BMBF Germany (Grant No. 06 MS 568 I TP4), Internationales Büro des BMBF (Grant Nos. X081.24 and 211.6), SCSR Poland (Grant Nos. 2P302 025 and 2P03B 88 08), a DAAD-Academy of Finland contract, and COSY Jülich is gratefully acknowledged.

[1] H. O. Meyer *et al.*, Nucl. Phys. **A539**, 633 (1992).
[2] G. A. Miller and P. Sauer, Phys. Rev. C **44**, R1725 (1992).
[3] H. Machner and J. Haidenbauer, J. Phys. G **25**, R231 (1998).
[4] A. Bondar *et al.*, Phys. Lett. B **356**, 8 (1995).
[5] J. Zlomanczuk *et al.*, Phys. Lett. B **436**, 251 (1998).
[6] R. Bilger *et al.*, Nucl. Phys. **A693**, 633 (2001).
[7] H. O. Meyer *et al.*, Phys. Rev. Lett. **81**, 3096 (1998).
[8] H. O. Meyer *et al.*, Phys. Rev. Lett. **83**, 5439 (1999).
[9] H. O. Meyer *et al.*, Phys. Rev. C **63**, 064002 (2001).
[10] G. Rappenecker *et al.*, Nucl. Phys. **A590**, 763 (1995).
[11] M. Betigeri *et al.*, Phys. Rev. C **63**, 044011 (2001).
[12] M. Betigeri *et al.*, Nucl. Instrum. Methods Phys. Res. A **421**, 447 (1999).
[13] M. Drochner *et al.*, Nucl. Phys. **A643**, 55 (1998).
[14] M. Betigeri *et al.*, Nucl. Phys. **A690**, 473 (2001).
[15] CERNLIB, 1998.
[16] H. Machner and B. Razen, Nucl. Instrum. Methods Phys. Res. A **437**, 419 (1999).
[17] D. S. Koltun and A. Reitan, Phys. Rev. **141**, 1413 (1966).
[18] J. Niskanen, Phys. Lett. **112B**, 17 (1982).
[19] J. A. Niskanen, Phys. Lett. B **289**, 227 (1992).
[20] J. A. Niskanen, Nucl. Phys. **A298**, 417 (1978).
[21] H. Machner, Nucl. Phys. **A633**, 633 (1998).
[22] M. Gell-Mann and K. M. Watson, Annu. Rev. Nucl. Part. Sci. **4**, 219 (1954).
[23] A. H. Rosenfeld, Phys. Rev. **96**, 139 (1954).
[24] H. P. Noyes, Annu. Rev. Nucl. Part. Sci. **22**, 465 (1972).
[25] C. Hanhart and K. Nakayama, Phys. Lett. B **454**, 176 (1999).
[26] J. A. Niskanen, Phys. Lett. B **456**, 107 (1999).
[27] C. Hanhart, Ph.D. thesis, University of Bonn, 1997.
[28] S. Stanislaus *et al.*, Phys. Rev. C **41**, R1913 (1990).
[29] F. Shimizu *et al.*, Nucl. Phys. **A386**, 571 (1982).
[30] V. Flaminio, W. G. Moorhead, D. R. O. Morrison, and N. Rivoire, Compilation of Cross Sections III, CERN-HERA 84-01, 1984.